Zeitschrift: IABSE reports of the working commissions = Rapports des commissions de travail AIPC = IVBH Berichte der Arbeitskommissionen

Band: 34 (1981)

Artikel: A fracture mechanics model for reinforced concrete collapse

Autor: Carpinteri, Alberto

DOI: https://doi.org/10.5169/seals-26877

A Fracture Mechanics Model for Reinforced Concrete Collapse

Un modèle de mécanique de rupture pour le béton armé.

Ein Bruchmechanikmodell für das Versagen von Stahlbeton.

ALBERTO CARPINTERI
Research Assistant,
University of Bologna,
Bologna, Italy.

SUMMARY
The Limit Analysis of reinforced concrete beams does not take into consideration the cracks which usually develop in concrete, and the consequent stiffness variation and stress concentration. In the present paper such effects will be studied on the basis of Fracture Mechanics concepts. Thus it will be shown how the stability of the process of concrete fracture and steel plastic flow depends on the mechanical and geometrical (scale included) properties of the beam cross-section.

RÉSUMÉ
L'analyse limite de la section d'une poutre en béton armé ne tient pas compte des fissures normalement produites dans le béton et les variations de rigidité et de concentration des contraintes. Dans cette note, on étudie ces effets sur la base des principes de la Mécanique de la Rupture. Par conséquent, on montre que la stabilité du phénomène de formation des fissures dans le béton et de la plasticité de l'acier, dépend des caractéristiques mécaniques et géométriques (y inclus l'échelle) de la section de la poutre examinée.

ZUSAMMENFASSUNG
Die Traglastberechnung eines Trägerquerschnitts aus Stahlbeton trägt keineswegs Rechnung met den Rissen, die in der Regel beim Beton auftreten, sowie den damit zusammenhängenden Steifigkeitsänderungen und Änderungen der Spannungskonzentration. Genannte Wirkungen werden in diesem Beitrag unter Zugrundelegung bruchmechanischer Begriffe untersucht. Es wird sich damit zeigen, inwieweit die stabile Rissausbreitung in Beton und das Fliessen des Stahls von den mechanischen und geometrischen (einschliesslich der Masstabs-) Eigenschaften des Querschnitts abhängig sind.

1. INTRODUCTION.

In the Limit Analysis of the reinforced concrete beam cross-section the stretched part of concrete is conventionally assumed not to be traction bearing, while a perfectly plastic behaviour of the compressed part is hypothesized [1]. Such analysis doesn't take into consideration the cracks, which usually develop in concrete and generally cause that more complex crisis phenomenon which is the collapse of the concrete-steel system. In fact the Limit Analysis approach doesn't consider the stiffness variation and the stress concentration due to the crack's presence at all. On the other hand these two effects can be taken and studied through Fracture Mechanics concepts.

By tradition the problems relating to cracked masonry or concrete constructions are studied on the basis of empirical parameters, such as the crack width, i.e. the distance between the crack free surfaces [2]. Such parameters cannot be considered as absolute indications of the crack stability condition, but only as alarm signals of incipient collapses. In fact the crack width will not be constant, but will generally increase, moving away from the crack tip. It will however depend on the sizes of the cracked structure. In the present treatment scale effects will be emphasized in the collapse phenomena of reinforced concrete beams, as has been already done for plain concrete structures [3] [4] [5] [6].

Four types of potential collapses will be considered:

1) concrete fracture collapse ($K_I \geqslant K_{IC}$);
2) concrete ultimate strength collapse ($\sigma \geqslant f_u$);
3) concrete crushing collapse ($\sigma \geqslant f_c$);
4) steel plastic flow collapse ($\sigma \geqslant f_y$).

The final collapse is generally the definitive and irreversible consequence of the four above mentioned collapses. Such collapses will occur in a well defined sequence, according to the mechanical and geometrical (scale included) properties of the beam cross-section. The only collapse, which, even though very frequent, will not be considered, is the slip between reinforcement and concrete.

Then the stability of the process of concrete fracture and steel plastic flow will be studied, and its dependence on the mechanical and geometrical (scale included) properties of the beam cross-section will be shown. A role of primary importance, besides that of steel percentage A_S/A [2], is played by the non-dimensional number $f_y b^{1/2}/K_{IC}$ (analogous to the Brittleness Number defined in [4]), which includes the mechanical properties of the materials and the sizes of the structure.

2. HYPERSTATIC REACTION OF REINFORCEMENT.

Consider a reinforced concrete beam segment, with a rectangular cross-section of thickness t and width b, subjected to a bending moment M. Let the steel reinforcement be distant h from the external surface, and a through-thickness edge crack of depth $a \geqslant h$ is assumed to exist in the stretched part (Fig. 1). Therefore the cracked concrete beam segment will be in all subjected to the external bending moment M and to an eccentric axial force F, due to the hyperstatic reaction of the reinforcement. It is well-known that a bending moment M* induces a stress-intensity factor K_I at the crack tip equal to:

$$K_I = \frac{M^*}{b^{3/2} t} Y_M(\xi), \tag{1}$$

where $\xi = a/b$ is the relative crack depth and Y_M is the function [7]:

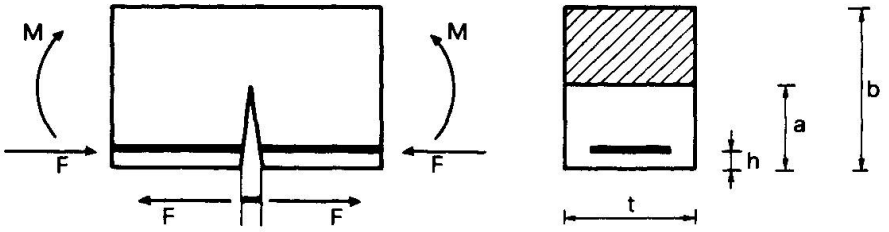

Fig. 1 Cracked reinforced beam segment.

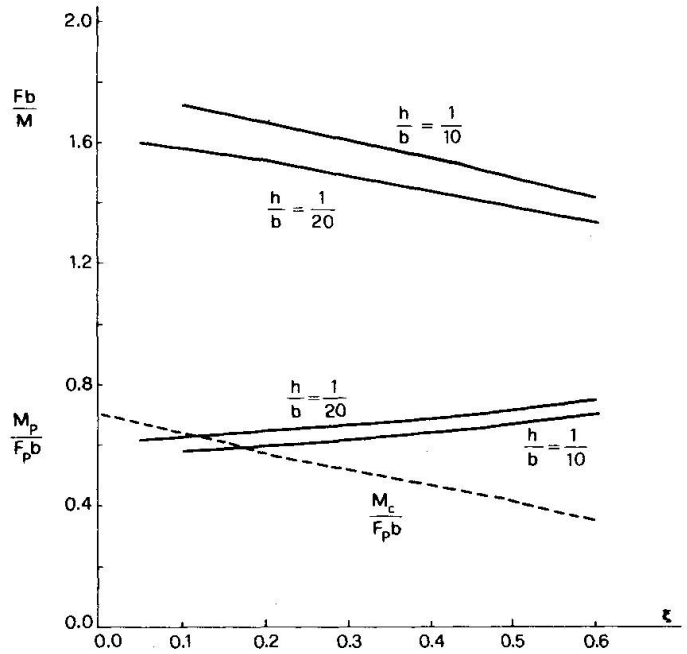

Fig. 2 Hyperstatic reaction of reinforcement and bending moment of reinforcement plastic flow.

$$Y_M(\xi) = 1.99\,\xi^{1/2} - 2.47\,\xi^{3/2} + 12.97\,\xi^{5/2} - 23.17\,\xi^{7/2} + 24.80\,\xi^{9/2}, \tag{2}$$

for $\xi \leqslant 0.6$.

In the same way, an axial tensile force F* induces the stress-intensity factor:

$$K_I = \frac{F^*}{b^{1/2}t}\,Y_F(\xi), \tag{3}$$

with [7]:

$$Y_F(\xi) = 1.99\,\xi^{1/2} - 0.41\,\xi^{3/2} + 18.70\,\xi^{5/2} - 38.48\,\xi^{7/2} + 53.85\,\xi^{9/2}, \quad \text{for } \xi \leqslant 0.6. \tag{4}$$

On the other hand the bending moment M* causes a relative rotation φ equal to [8] [9]:

$$\varphi = \lambda_{MM}\,M^*, \tag{5}$$

with:

$$\lambda_{MM} = \frac{1}{b^2 t E}\int_0^{\xi} Y_M^2(\xi)\,d\xi, \tag{6}$$

while the axial tensile force F* causes the rotation [8] [9]:

$$\varphi = \lambda_{MF} F^*, \tag{7}$$

with:
$$\lambda_{MF} = \frac{1}{btE} \int_0^{\xi} Y_M(\xi)\, Y_F(\xi)\, d\xi. \tag{8}$$

In the case of the considered statically indeterminate system, i.e. the reinforced beam segment (Fig.1), the global moment acting on the cross-section will be:

$$M^* = M - F\left(\frac{b}{2} - h\right), \tag{9}$$

that is, it will be given by the external moment, opening the crack, subtracted by the reinforcement reaction moment, closing the crack. Then the axial force acting on the cross-section will be:

$$F^* = -F. \tag{10}$$

Up to the moment of steel yielding, the global rotation, due to the bending moment M* and to the closing force F*, will be zero:

$$\varphi = \lambda_{MM} M^* + \lambda_{MF} F^* = 0. \tag{11}$$

The equation (11) is the congruence condition able to provide the hyperstatic unknown F. Namely, replacing the expressions (9) and (10) in (11), the result is:

$$\lambda_{MM}\left[M - F\left(\frac{b}{2} - h\right)\right] - \lambda_{MF} F = 0, \tag{12}$$

and finally it is possible to obtain:

$$\frac{Fb}{M} = \frac{1}{\left(\frac{1}{2} - \frac{h}{b}\right) + r(\xi)}, \tag{13}$$

where:

$$r(\xi) = \frac{\int_0^{\xi} Y_M(\xi)\, Y_F(\xi)\, d\xi}{\int_0^{\xi} Y_M^2(\xi)\, d\xi}. \tag{14}$$

The hyperstatic reaction of the reinforcement, against the relative crack depth, for h/b = 1/10, 1/20 , is reported in the diagram of Figure 2. The decrease of the hyperstatic reaction by increasing the crack depth is not intuitive, and indeed it may even surprise the reader. However it can be explained by observing that the compliances λ_{MM} and λ_{MF} both increase by increasing the crack length, but λ_{MF} increases more rapidly than λ_{MM} does. Thus lower and lower axial forces F are needed to annul the rotation due to the external moment M.

3. BENDING MOMENT OF REINFORCEMENT PLASTIC FLOW.

As the expression (13) shows, the force F, transmitted by the reinforcement, increases linearly by increasing the external moment M, until the limit force $F_p = f_y A_s$ is reached, being f_y the steel yield strength and A_s the steel area. From this point onwards a perfectly plastic behaviour of the reinforcement will be considered. It means that the infinitesimal reinforcement segment, which is uncovered, i.e. included between the two crack surfaces, will flow, always transmitting the same force F_p to the cracked concrete segment (Fig. 3).

From (13) it is possible to obtain the moment of plastic flow for the reinforcement:

$$M_p = F_p b \left[\left(\frac{1}{2} - \frac{h}{b}\right) + r(\xi)\right]. \tag{15}$$

Such moment against the relative crack depth, for $h/b = 1/10, 1/20$, is reported in Figure 2. According to the hyperstatic force decrease by increasing the crack depth ξ (Fig. 2), an increase of the moment of reinforcement plastic flow M_p occurs by increasing ξ.

However it is necessary to observe that, if concrete presents a low crushing strength f_c and steel a relatively high yield strength f_y, the concrete crushing collapse can come before the steel plastic flow. If M_c is the external moment of concrete crushing and a hypothesis of linear stress variation through the ligament holds (Fig. 4) [2], it results:

$$\frac{M_c}{F_p b} = \frac{f_c}{f_y \dfrac{A_s}{A}} \cdot \frac{(1-\xi)\left(2+\xi-3\dfrac{h}{b}\right)}{6}. \tag{16}$$

The dashed line of Figure 2 represents the diagram of function (16) for $f_c = 200$ kg cm^{-2}, $f_y = 3600$ kg cm^{-2}, $A_s/A = 0.024$ and $h/b = 1/10$. It can be observed that, although values very favourable to the concrete crushing collapse have been chosen, such collapse in fact comes before the steel plastic flow only for sufficiently high values of the crack depth ($\xi \geqslant 0.175$).

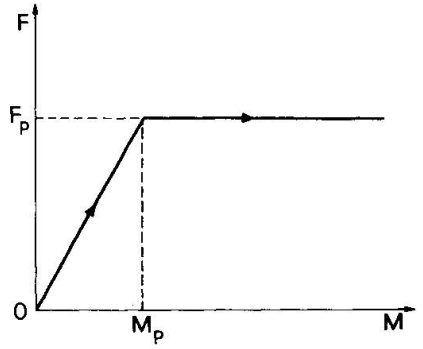

Fig. 3 Hyperstatic force transmitted by the reinforcement against the applied moment.

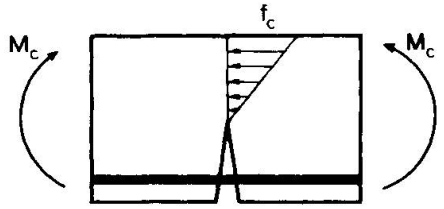

Fig. 4 Hypothesis of linear stress variation through the ligament.

4. RIGID-HARDENING BEHAVIOUR OF THE CRACKED BEAM SEGMENT.

The purpose of the present section is to describe the mechanical behaviour of the cracked reinforced

concrete beam segment, once the bending moment M_p of steel plastic flow has been exceeded. For $M \leqslant M_p$ we have namely $\varphi = 0$, while for $M > M_p$:

$$\varphi = \lambda_{MM}\left[M - F_p\left(\frac{b}{2} - h\right)\right] - \lambda_{MF} F_p. \tag{17}$$

The $M - \varphi$ diagram for the cracked beam segment is represented in Figure 5. This diagram expresses the equivalence of the beam segment with a rigid-linear hardening spring. It is interesting to observe how the hardening line is parallel to the $M - \varphi$ diagram relating to the same cracked beam segment without reinforcement (broken line).

The hardening coefficient λ_{MM}^{-1} against the relative crack depth ξ is reported in Figure 5 again. By increasing the crack depth ξ, the hardening line becomes more and more inclined, until giving rigid--perfectly plastic behaviour. On the other hand, for $\xi \to 0$, the hardening line becomes nearly vertical, until giving a rigid behaviour of the beam segment simulating spring.

Therefore, summarizing, one can conclude that, by increasing ξ, the moment of steel plastic flow increases (Fig. 2), while the slope of the hardening line decreases (Fig. 5). Some $M - \varphi$ diagrams, for $h/b = 1/20$, are reported in Figure 6, varying ξ between 0.05 and 0.50. The moment of steel plastic flow increases very little by increasing ξ; on the other hand the slope of the hardening line decreases sharply.

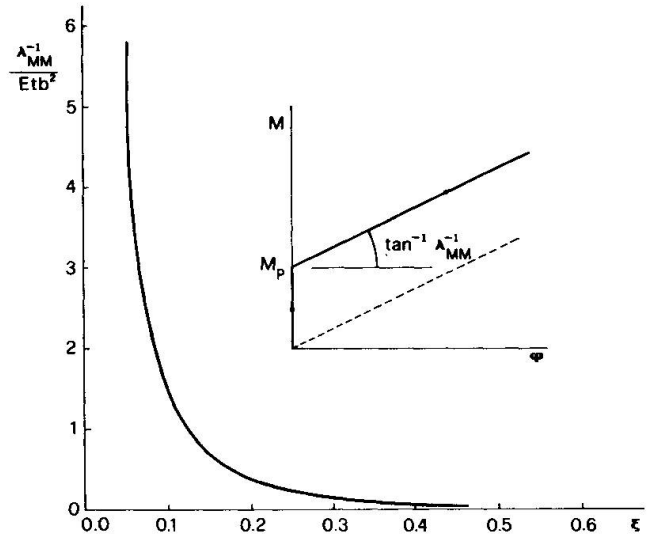

Fig. 5 Hardening coefficient against relative crack depth.

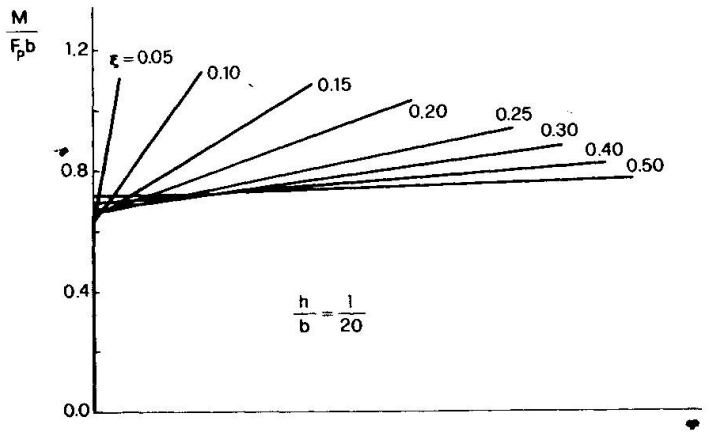

Fig. 6 Moment-rotation diagrams for different crack depths.

5. BENDING MOMENT OF CONCRETE FRACTURE.

In the preceding section the behaviour of the cracked beam segment has been considered, for bending moments higher than the steel plastic flow moment M_p. In the present section the concrete fracture collapse will be examined, which is consequent to the steel plastic flow collapse, i.e. it occurs for a bending moment $M_F \geqslant M_p$.

After the steel plastic flow, the stress-intensity factor acting at the crack tip will be equal to the algebraical addition of the factors (1) and (3), and the actual loadings will be:

$$M^* = M - F_p\left(\frac{b}{2} - h\right), \tag{18}$$

$$F^* = -F_p\,. \tag{19}$$

Thus it will be:

$$K_I = \frac{1}{b^{3/2}t}\,Y_M(\xi)\left[M - F_p\left(\frac{b}{2} - h\right)\right] - \frac{F_p}{b^{1/2}t}\,Y_F(\xi). \tag{20}$$

Presuming the expression (20) to be equal to the concrete fracture toughness K_{IC}, it is possible to obtain the fracture moment M_F:

$$M_F = \frac{K_{IC}b^{3/2}t}{Y_M(\xi)} + \frac{F_p b}{Y_M(\xi)}\left[Y_F(\xi) + Y_M(\xi)\left(\frac{1}{2} - \frac{h}{b}\right)\right]. \tag{21}$$

In non-dimensional form:

$$\frac{M_F}{K_{IC}b^{3/2}t} = \frac{1}{Y_M(\xi)} + N_p\left[\frac{Y_F(\xi)}{Y_M(\xi)} + \frac{1}{2} - \frac{h}{b}\right],$$

where:

$$N_p = \frac{f_y b^{1/2}}{K_{IC}} \cdot \frac{A_s}{A}\,. \tag{22}$$

The concrete fracture moment M_F against the relative crack depth ξ is reported in Figure 7, varying the non-dimensional number N_p (h/b = 1/20).

For N_p values close to zero, that is for low reinforced beams (either, for aggregative materials with high K_{IC}, or for very small cross-sections), the fracture moment decreases while the crack extends, and then a typical phenomenon of unstable fracture occurs.

For higher N_p values, a stable branch follows the unstable one of the curve, which describes the crack extension against the applied load. Already for $N_p = 1$ the minimum of the curve is evident and takes place for $\xi \simeq 0.35$. For higher N_p values, the ξ value, for which the minimum occurs, is lower, while the stable branch becomes steeper and steeper. For $N_p \gtrsim 8.5$ the unstable branch completely disappears and only the stable branch remains.

Analogous behaviour has been underlined in the case of a cracked masonry wall, subjected to an eccentric axial compression force [10]. However in that case the unstable branch and the consequent stable one appear steeper and the existence of the minimum is then more evident.

The locus minimorum is represented by a dashed line in Figure 7. This line divides the quadrant of the diagram into two zones: the upper zone is where the fracturing process is stable, while the lower one is where the process is unstable. Therefore, it is possible to assert that the fracturing process in reinforced concrete becomes stable only when the beam is sufficiently reinforced (either, when the

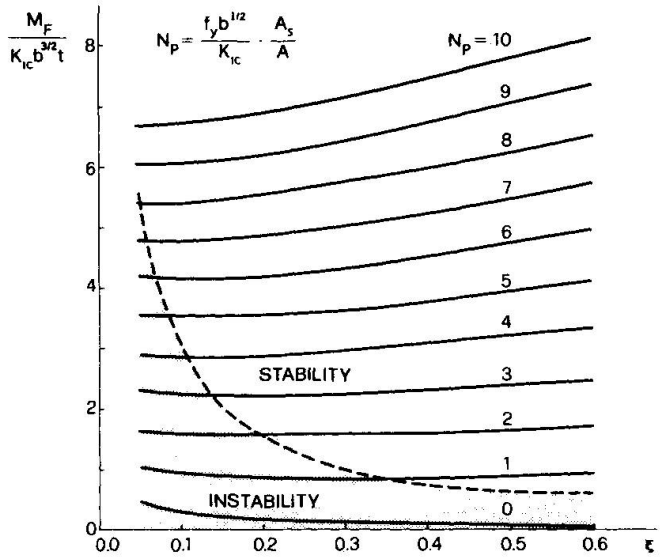

Fig. 7 Bending moment of concrete fracture against relative crack depth (h/b = 1/20).

fracture toughness K_{IC} is sufficiently low, or when the cross-section is sufficiently large), and when the crack is sufficiently deep.

If the curve N_p = constant were perfectly horizontal, a condition of indifferent equilibrium would occur. In fact none of the curves shows such a regularity. However it is important to observe how the curve relating to $N_p = 1$, which could represent the fracturing phenomenon for very common reinforced concrete beams, is only slightly deflected downwards. In fact the minimum is only about 15% lower than the value of the function for $\xi = h/b = 0.05$.

For h/b = 1/10 curves very similar to those of Figure 7 are obtained. Only two slight differences are present:

1) the curves go down, i.e. fracture collapse occurs for lower moments, since the reinforcement, being internal, resists to a lesser extent than in the preceding case;

2) the dashed line goes up, i.e. the stable zone of the diagram shrinks.

Finally it may be interesting to compute the non-dimensional number N_p for three different reinforced concrete beams. As a first example, consider the following set of values:

$$f_y = 2400 \text{ kg cm}^{-2}, \qquad K_{IC} = 80 \text{ kg cm}^{-3/2},$$
$$b = 30 \text{ cm}, \qquad A_s/A = 0.01,$$

from which one obtains:

$$N_P = \frac{f_y b^{1/2}}{K_{IC}} \cdot \frac{A_s}{A} = \frac{2400 \times 30^{1/2}}{80} \times 0.01 = 1.64.$$

Thus, it is possible to verify in the diagram of Figure 7, how, for this very common reinforced concrete beam, the fracturing process is very close to a condition of indifferent equilibrium.

Secondly, examine a low reinforced beam with small cross-section:

$$f_y = 2400 \text{ kg cm}^{-2}, \qquad K_{IC} = 100 \text{ kg cm}^{-3/2},$$
$$b = 20 \text{ cm}, \qquad A_s/A = 0.0024,$$

from which follows:

$$N_P = \frac{f_y b^{1/2}}{K_{Ic}} \cdot \frac{A_s}{A} = \frac{2400 \times 20^{1/2}}{100} \times 0.0024 = 0.26.$$

In this beam the fracturing process occurs in an unstable manner (Fig. 7).
As a third and last case, examine a high reinforced beam with large cross-section:

$$f_y = 3600 \text{ kg cm}^{-2}, \qquad K_{Ic} = 50 \text{ kg cm}^{-3/2},$$
$$b = 150 \text{ cm}, \qquad A_s/A = 0.0240,$$

from which it results:

$$N_P = \frac{f_y b^{1/2}}{K_{Ic}} \cdot \frac{A_s}{A} = \frac{3600 \times 150^{1/2}}{50} \times 0.0240 = 21.16.$$

In this beam the fracturing process occurs in a stable manner (Fig. 7).

6. STABILITY OF THE PROCESS OF CONCRETE FRACTURE AND STEEL PLASTIC FLOW.

In section 5 the stability of reinforced concrete fracturing process has been described on the basis of the curve representing the crack depth against the applied bending moment. In the present section such stability will be studied using energetic considerations.
The stress-intensity factor acting on the crack is:

$$K_I = \frac{1}{b^{3/2} t} Y_M(\xi) \left[M - F\left(\frac{b}{2} - h\right) \right] - \frac{1}{b^{1/2} t} Y_F(\xi) F, \quad \text{for } M \leqslant M_P, \tag{23}$$

$$K_I = \frac{1}{b^{3/2} t} Y_M(\xi) \left[M - F_P\left(\frac{b}{2} - h\right) \right] - \frac{1}{b^{1/2} t} Y_F(\xi) F_P, \quad \text{for } M > M_P. \tag{24}$$

Replacing expression (13) in (23), it results:

$$K_I = \frac{1}{b^{3/2} t} Y_M(\xi) \left[M - \frac{M}{b} \frac{1}{\left(\frac{1}{2} - \frac{h}{b}\right) + r(\xi)} \left(\frac{b}{2} - h\right) \right] -$$

$$- \frac{1}{b^{1/2} t} Y_F(\xi) \frac{M}{b} \frac{1}{\left(\frac{1}{2} - \frac{h}{b}\right) + r(\xi)}, \quad \text{for } M \leqslant M_P. \tag{25}$$

The equations (25) and (24) in non-dimensional form appear as follows:

$$\frac{K_I b^{1/2} t}{F_P} = Y_M(\xi) \frac{M}{F_P b} \left[1 - \frac{1}{1 + \frac{r(\xi)}{\left(\frac{1}{2} - \frac{h}{b}\right)}} \right] - \frac{M}{F_P b} Y_F(\xi) \frac{1}{\left(\frac{1}{2} - \frac{h}{b}\right) + r(\xi)}$$

$$\text{for } M \leqslant M_P, \tag{26}$$

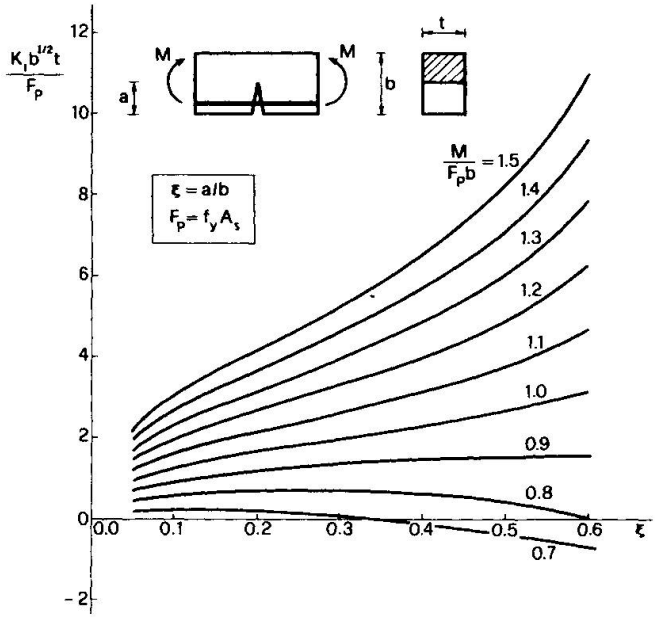

Fig. 8 Stress-intensity factor against relative crack depth, varying the applied moment (h/b = 1/20).

$$\frac{K_I b^{1/2} t}{F_p} = Y_M(\xi)\left[\frac{M}{F_p b} - \left(\frac{1}{2} - \frac{h}{b}\right)\right] - Y_F(\xi), \quad \text{for } M > M_p. \tag{27}$$

The stress-intensity factor K_I against the crack depth ξ is reported in Figure 8, varying the loading parameter $M/F_p b$ (h/b = 1/20). For $M/F_p b$ values lower than about 0.7, the stress-intensity factor is very low for every considered depth $h/b \leq \xi \leq 0.6$. As the curve $M/F_p b = 0.7$ clearly shows, the K_I value is positive for small depths ξ, while it becomes negative for larger depths. This means that, for $0 \leq M/F_p b \leq 0.8$ and sufficiently deep cracks, the assumed model predicts the closing of the crack, as well as the non-plastic state of steel. The plastic limit, as the diagram of Figure 2 suggests, is very near the curve $M/F_p b = 0.7$ reported in Figure 8. . More precisely it is included between the two curves $M/F_p b = 0.60$ and $M/F_p b = 0.75$.

For $M/F_p b > 0.8$ the K_I factor is positive for every investigated depth ξ. For $M/F_p b \gtrsim 0.9$ the K_I factor monotonicly increases as a function of the crack depth ξ. For $M/F_p b \lesssim 0.9$ the function $K_I(\xi)$ presents a positive maximum. This means that, for sufficiently low bending moments and sufficiently deep cracks, the fracturing process is stable. In fact, from an energetic point of view, one can assert that the generalized crack extension force $\mathcal{G}_I = K_I^2/E$ has the same course of K_I, for $M/F_p b > 0.8$. Thus for $0.8 \lesssim M/F_p b \lesssim 0.9$ and for sufficiently high ξ, it results:

$$\frac{\partial \mathcal{G}_I}{\partial \xi} = -\frac{\partial^2 V}{\partial \xi^2} < 0, \tag{28}$$

where V is the total potential energy of the concrete-steel system. That is, for those particular values of the bending moment and the crack depth, the total potential energy V can present, as a stationary point ($K_I = K_{IC}$), only a minimum and therefore a stable equilibrium condition.

7. FRACTURE SENSITIVITY INCREASE DUE TO REINFORCEMENT.

Up to now the only fact that has been clarified is that the concrete fracture collapse follows the reinforcement plastic collapse, and that, between the two mentioned collapses, the mechanical behaviour of the cracked beam segment is linear hardening. However no indication of how much the fracture moment M_F is higher than the plastic flow moment M_P has been given yet.
From (15) and (21) it follows:

$$\frac{M_P}{M_F} = \frac{\left[\frac{1}{2} - \frac{h}{b} + r(\xi)\right] Y_M(\xi)}{\frac{1}{N_P} + Y_F(\xi) + Y_M(\xi)\left(\frac{1}{2} - \frac{h}{b}\right)} \tag{29}$$

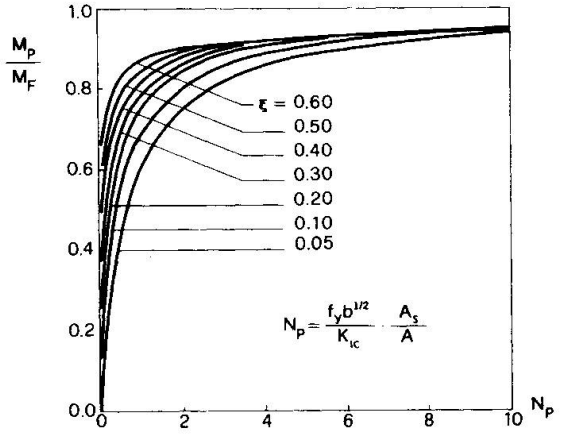

Fig. 9 Ratio between the moment of steel plastic flow and the moment of concrete fracture against the non-dimensional number N_p, varying the relative crack depth ξ (h/b = 1/20).

In Figure 9 the ratio M_P/M_F against the non-dimensional number N_p is represented, varying the crack depth ξ (h/b = 1/20). From this diagram one deduces that, the higher the number N_p and the deeper the crack, the closer the fracture collapse is to the plastic one. It means that the fracture collapse can be obtained immediately after the plastic one, particularly by varying two parameters:
1) by increasing the beam size b;
2) by increasing the steel percentage A_s/A.
Of the four potential collapses mentioned in the Introduction, only three have been explicitly considered up to now. In section 3 it has been said that the concrete crushing collapse tends to precede the others for high steel percentages A_s/A, as equation (16) shows. Once such collapse has been avoided, the other three are to be considered. The steel plastic collapse is certainly the first to be reached, while the ultimate strength collapse and the fracture collapse of concrete follow with a priority which is difficult to estimate.

8. SYNTHESIS AND CONCLUDING REMARKS.

In Figure 10 the diagrams moment-rotation $M(\varphi)$ are reported for h/b = 1/20, $\xi = 0.1$ and for five

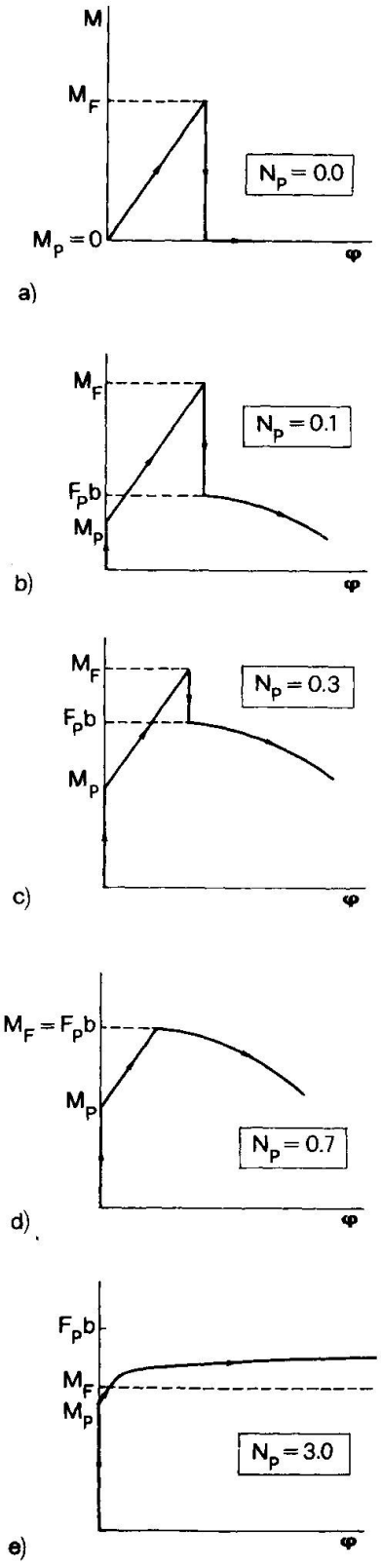

Fig. 10 Mechanical behaviour of the cracked reinforced beam segment, for different non-dimensional numbers N_p ($h/b = 0.05$; $\xi = 0.10$).

different values of number N_p: 0.0, 0.1, 0.3, 0.7, 3.0. Once the cross-section sizes and the mechanical properties of the material have been defined, they represent five different steel areas.

Rigid behaviour ($0 \leqslant M \leqslant M_p$) is followed by linear hardening behaviour ($M_p < M \leqslant M_F$). The latter stops when the concrete fracture collapse occurs. If the fracture phenomenon is unstable (section 5), function $M(\varphi)$ presents a discontinuity and drops from the value M_F to the value F_pb with a negative jump (Figs. 10-a, b, c, d). In fact in this case a complete and instantaneous disconnection of the concrete cross-section occurs. While the rotation φ is constant, the new moment F_pb can be estimated according to the scheme of Figure 11, where each beam segment is subjected to the traction F_p of the reinforcement and to the contact compression F_p, i.e. altogether, to the moment $F_p(b - h) \simeq F_pb$. Then, increasing the rotation φ and lacking any phenomenon of instability, the bending moment decreases with a non-linear law (Fig. 11):

$$M = F_pb \cos\frac{\varphi}{2}. \tag{30}$$

On the other hand, if the fracture phenomenon is stable, function $M(\varphi)$ doesn't present any discontinuity and describes hardening behaviour (Fig. 10-e) analogous to that of Figure 6.

In Figure 10-a the case $N_p = 0$ is considered, i.e. the beam without reinforcement. The plastic flow moment M_p is naturally equal to zero, as well as the moment F_pb, which occurs immediately after the complete disconnection of concrete.

In figure 10-b the case $N_p = 0.1$ is described, i.e. a low reinforced beam. By the diagram of Figure 2 it is possible to obtain the ratio M_p/F_pb, while by the diagram of Figure 9 the ratio M_p/M_F. The slope of the hardening line doesn't vary with respect to the preceding case, since it depends only on the crack length, besides the concrete elastic modulus and the cross-section sizes (Fig. 5).

In Figure 10-c the case $N_p = 0.3$ is considered, which is analogous to the previous one, except for the fact that the ratio M_p/M_F is higher. On the other hand the ratio M_p/F_pb, which is independent of N_p (Fig. 2), remains unchanged.

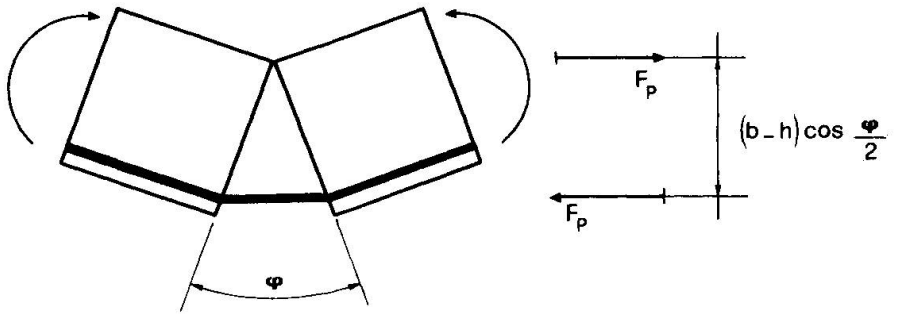

Fig. 11 Statical scheme after the complete disconnection of concrete.

In Figure 10-d the case $N_p = 0.7$ is reported. For this value it is $M_F = F_p b$, and then the discontinuity vanishes.

Finally in Figure 10-e the case $N_p = 3$ is described. In this case the fracture moment M_F is only slightly higher than the plastic moment M_p, and the moment $F_p b$ would be obtainable only with a positive jump of the function. On the other hand, from Figure 7 it is known that the fracturing process, for $N_p = 3$ and $\xi \geqslant 0.14$, is stable, and thus a complete and instantaneous disconnection of concrete can not occur (Fig. 11).

It is observed that, as for $N_p \leqslant 0.7$ it is $F_p b \leqslant M_F$, and then a discontinuity appears in the diagram $M(\varphi)$ (Figs. 10-a, b, c, d), so for $N_p \leqslant 0.7$ the curves of Figure 7 lie completely in the unstable zone.

Therefore it is possible to conclude that, by increasing the steel percentage A_s/A, or, in the same way, by increasing the beam size b, the concrete fracturing process becomes stable. In the meantime, as has been shown in section 7, the fracture sensitivity of the system increases.

ACKNOWLEDGMENTS

The author gratefully acknowledges the research support of the Italian National Research Council (C.N.R.).

REFERENCES.

[1] "Raccomandazioni CEB/FIP per le strutture in cemento armato", Edizione italiana A.I.T.E.C.

[2] AVRAM, C., FILIMON, I., DEUTSCH, I., CLIPII, T.: "Crack control and crack widths in low reinforced concrete members", Corso di Perfezionamento per le Costruzioni in Cemento Armato "Fratelli Pesenti", Politecnico di Milano, 1979, pp. 295 - 319.

[3] CARPINTERI, A. : "Size effect in fracture toughness testing: a Dimensional Analysis approach", Proceedings International Conference on Analytical and Experimental Fracture Mechanics, Ed. G.C. Sih, Roma, 1980.

[4] CARPINTERI, A.: "Notch sensitivity in fracture testing of aggregative materials", Engineering Fracture Mechanics, to appear.

[5] CARPINTERI, A.: "Experimental determination of fracture toughness parameters K_{IC} and J_{IC} for aggregative materials", Proceedings 5th International Conference on Fracture, Cannes, 1981.

[6] CARPINTERI, A.: "Static and energetic fracture parameters for rocks and concretes", Materials and Structures (RILEM), to appear.

[7] OKAMURA, H., WATANABE, K., TAKANO, T.: "Applications of the compliance concept in Fracture Mechanics", ASTM STP 536, 1973, pp. 423 - 438.

[8] OKAMURA, H., WATANABE, K., TAKANO, T.: "Deformation and strength of cracked member under bending moment and axial force", Engineering Fracture Mechanics, 1975, Vol. 7, pp. 531-539.

[9] CARPINTERI, A., DI TOMMASO, A., VIOLA, E.: "Fatigue evolution of multicracked frame--structures", Proceedings International Conference on Analytical and Experimental Fracture Mechanics, Ed. G.C. Sih, Roma, 1980.

[10] CARPINTERI, A., DI TOMMASO, A., VIOLA, E.: "Sulla capacità portante limite di pareti lapidee lesionate", Atti del 5° Congresso AIMETA, Associazione Italiana Meccanica Teorica e Applicata, Palermo, 1980.